Since January 2020 Elsevier has created a COVID-19 resource centre with free information in English and Mandarin on the novel coronavirus COVID-19. The COVID-19 resource centre is hosted on Elsevier Connect, the company's public news and information website.

International Journal of Biological Macromolecules 162 (2020) 11–23

Contents lists available at ScienceDirect

International Journal of Biological Macromolecules

journal homepage: http://www.elsevier.com/locate/ijbiomac

Comparative studies of the expression of creatine kinase isoforms under immune stress in *Pelodiscus sinensis*

Caiyan Li [a,1], Wei Wang [a,1], Jinhyuk Lee [b], Lifang Zeng [a], Yufei Yang [a], Shang-Jun Yin [a], Yong-Doo Park [a,c,*], Guo-Ying Qian [a,**]

[a] College of Biological and Environmental Sciences, Zhejiang Wanli University, Ningbo 315100, PR China
[b] Genome Editing Research Center, Korea Research Institute of Bioscience and Biotechnology (KRIBB), Gwahak-ro, Yuseong-gu, Daejeon 34141, Republic of Korea
[c] Skin Diseases Research Center, Yangtze Delta Region Institute of Tsinghua University, 705 Yatai Road, Jiaxing 314006, PR China

ARTICLE INFO

Article history:
Received 15 May 2020
Received in revised form 4 June 2020
Accepted 4 June 2020
Available online 9 June 2020

Keywords:
Creatine kinase
Pelodiscus sinensis
Immune stress

ABSTRACT

The expression and localization of different isoforms of creatine kinase in *Pelodiscus sinensis* (PSCK) were studied to reveal the role of PSCK isozymes (PSCK-B, PSCK-M, PSCK-S) under bacterial infection-induced immunologic stress. The computational molecular dynamics simulations predicted that PSCK-S would mostly possess a kinase function in a structural aspect when compared to PSCK-B and PSCK-M. The assay of biochemical parameters such as total superoxide dismutase (T-SOD), lactate dehydrogenase (LDH), malondialdehyde (MDA), catalase (CAT), and the content of ATP were measured along with total PSCK activity in different tissue samples under bacterial infection. The expression detections of PSCK isozymes *in vitro* and *in vivo* were overall well-matched where PSCK isozymes were expressed differently in *P. sinensis* tissues. The results showed that PSCK-B mostly contributes to the spleen, followed by the liver and myocardium; PSCK-M mostly contributes to the liver, followed by the myocardium and skeletal muscle, while PSCK-S contributes to the spleen and is uniquely expressed in skeletal muscle. Our study suggests that the various alterations of PSCK isozymes in tissues of *P. sinensis* are prone to defense the bacterial infection and blocking energetic imbalance before severe pathogenesis turned on in *P. sinensis*.

1. Introduction

Creatine kinase (CK, alias creatine phosphokinase) is the key enzyme of ATP metabolism in animal cells. It exists mainly in skeletal muscle and the myocardium, to a lesser extent in brain tissue, and a small amount in smooth muscle, red blood cells and the liver where it catalyzes the phosphorylation of creatine [1–3]. It is generally recognized that CK has dimeric subunits that exist as isoenzymes with the greatest activity in muscle (CK-MM), the heart (CK-MB), and the brain (CK-BB). An additional form of the CK enzyme exists in mitochondria (CK-Mt), compared to cytosolic forms [4,5], of which there are two types of isoenzymes — ubiquitous (CK-U) and sarcomeric (CK-S). CK-S is located in the outer region of the granular body and mainly expressed in muscle tissue while CK-U is expressed in many types of cells and tissues. The distribution of the CK isoenzyme therefore varies between tissues and species.

The CK system in animal cells and associated pleiotropic effects of creatine as a typical substrate of CK [6,7] has been well documented. A primary role of CK has been identified in the maintenance of ADP homeostasis, the regulation of phospho-creatine (PCr) and general CK-PCr system-induced functions, as well as the importance of creatine supplementation as a nutrient. Furthermore, the physiological function of creatine and the relationship of creatine, neuroprotection, and cognitive functions have been documented, suggesting that creatine could be used as a metabolic agent [8]. In terms of immune response, CK was associated with metabolic changes in the severity of hand, foot and mouth disease (HFMD). CK and the isoenzyme CK-MB were significantly reduced in the peripheral blood of severe cases and thus a decreased level of CK in peripheral blood was suggested as a predictor of severe HFMD [9]. CK isoenzymes also play important roles directly related to the occurrence of various diseases. For instance, a low level of CK in serum is associated with an increased risk of death in chronic kidney disease [10] and a significant decrease in the serum ubiquitous CK-Mt activity in Parkinson's disease patients [11]. In infectious diseases, CK

Abbreviations: CK, creatine kinase; PSCK, CK from *Pelodiscus sinensis*; PSCK-B, brain type of PSCK; PSCK-M, muscle type of PSCK; PSCK-S, mitochondrial sarcomeric type of PSCK (type II); ADP, adenosine diphosphate; ATP, adenosine triphosphate; MD, molecular dynamics; ps, picosecond; ns, nanosecond; T-SOD, total superoxide dismutase; LDH, lactate dehydrogenase; MDA, malondialdehyde; CAT, catalase; IHC, immunohistochemistry; RT-PCR, reverse transcription polymerase chain reaction; RACE, rapid-amplification of cDNA ends.

* Correspondence to: Y-D. Park, B-18F, No. 705 Yatai Road, Nanhu District, Jiaxing 314006, Zhejiang, PR China.
** Correspondence to: G-Y. Qian, No. 8 Qianhu South Road, Yinzhou District, Ningbo 315100, Zhejiang, PR China.
E-mail addresses: parkyd@hotmail.com (Y.-D. Park), qiangy@zwu.edu.cn (G.-Y. Qian).
[1]These authors contributed equally to this study.

https://doi.org/10.1016/j.ijbiomac.2020.06.036
0141-8130/

was detected as upregulated in severe acute respiratory syndrome (SARS) [12], and was also found to be increased in corona virus disease 2019 (COVID-19) [13]. An earlier report showed that the elevation of CK is connected to disease severity in H7N9 infection [14].

There have been few mitochondrial types of CK isolated in reptiles until now, of which mitochondrial type I (CK-U) and type II (CK-S) have been isolated from various sources of reptiles as listed in Supplementary Table 1. Two mitochondrial isoforms from *Alligator sinensis*, *Pogona vitticeps* (central bearded dragon), *Alligator mississippiensis* (American alligator), and *Anolis carolinensis* have been reported, and only one type of mitochondrial isoform has been isolated from *Gavialis gangeticus* (Gharial), *Crocodylus porosus* (Australian saltwater crocodile), *Gekko japonicas*, and *Pelodiscus sinensis* (Chinese soft-shelled turtle). However, CK isoforms from reptiles are rarely reported compared to mammalians. Previously we have reported two isoforms of CK from *P. sinensis* (PSCK-B and PSCK-M) — GenBank accession No. JQ410386.1 and KR633145.1 respectively [15,16], analyzed by RACE technique. As a sequential study, we have analyzed the mitochondrial isoform of *P. sinensis* identified as type II mitochondrial isoform (PSCK-S), listed in Supplementary Table 1. Our research group also previously submitted PSCK-S to GenBank and registered the accession No. as MF374343.1.

In the present study we compared the expression and localization of three different subtypes of PSCK (PSCK-B, PSCK-M, PSCK-S) under immune stress. We found that isoforms of PSCK functioned in different tissues in response to immune challenge. It is indicative that the PSCK-creatine (phosphor-creatine) system on the ATP-consuming or generating process in the flow of energy metabolism, is directly linked to the immune response in *P. sinensis*. The Chinese soft-shelled turtle is a unique economic aquatic animal in China, very sensitive to stress, and our study provides informative data for both understanding the metabolic enzyme of *P. sinensis* and for agricultural purposes.

2. Materials and methods

2.1. Turtle breeding and bacterial infection

Healthy and unwounded Chinese soft-shelled turtles (*P. sinensis*) weighing between 200 and 250 g were obtained from a turtle culture farm in Ningbo City in September. These turtles were kept separately in an automatic control aquarium system in Zhejiang Wanli University. The turtles showed no clinical signs or laboratory evidence of the *Aeromonas* genus or other infections. After two weeks of pre-breeding, ten turtles were intraperitoneally injected with freshly prepared *A. hydrophila* T4 strain (kindly provided by Prof. Chengping Lu, Nanjing Agriculture University) in a single dose of 1.0×10^8 CFU/50 g body weight (injected group, IG). Another ten were injected with sterilized saline solution (control group, CG). Before injection, the T4 strain had already been through the regression tests, and the results showed all turtles presented the same symptoms and necropsy as the natural case.

The ethical standards of experimental protocols involving live animals were in accordance with the Guide for the Care and Use of Laboratory Animals prepared by the Institutional Animal Care and Use Committee of Zhejiang Wanli University and all procedures were approved by this same committee.

2.2. Sample preservation and RNA preparation

The turtles were euthanized 24 h post-challenge and tissues of the myocardium, liver, spleen, kidney, and skeletal muscle were collected and washed with DEPC treated saline. Half of the samples were frozen in liquid nitrogen and stored at −80 °C for molecular biological detection, and the other half cleared and fixed with 10% formaldehyde solution for 48 h for histological studies. The total RNA was extracted from these frozen tissues using Trizol reagent (Invitrogen) according to the manufacturer's instructions.

2.3. Cloning of PSCK-S and bioinformatic analysis

The sequence of PSCK-S containing the whole CDS (coding region) was obtained from the transcriptome sequencing data of *P. sinensis* in our previous study [17], in which de-novo characterization of the soft-shelled turtle (*P. sinensis*) transcriptome was performed using Illumina RNA-Seq technology. The gene was defined by overlap PCR amplification and splicing was performed after positive and negative monoclonal sequencing. The primers for forward and reverse were designed as PSCK-S Primer 1, 1F (5′-TTT ATG CTT CTG GGC TCG-3′) and 1R (5′-GGA GAC ACT GGC TTA TCA A-3′); and PSCK-S Primer 2, 2F (5′-ATA TTA TAG CCT GAC CAA-3′) and 2R (5′-TTA ATC ATC TGT AAC AAG C-3′), using OLIGO 7 Primer Analysis Software [18]. The sizes of amplified products were estimated at 774 bp and 662 bp respectively and the splicing sequence was identified with the BLAST program (https://blast.ncbi.nlm.nih.gov/Blast.cgi).

For bioinformatic analysis, the translated amino acids were used to search homologue sequences of CK-S in the NCBI database, and sequences were selected by the parameters (Query cover = 100%; E value = 0; and Identities >85%). Based on BLAST pairwise alignment, the NJ (Neighbor Joining) tree was created. To identify structural differentiation among three PSCK (PSCK-B, PSCK-M, PSCK-S), multiple sequence alignment was performed using program Clustal W [19]. The molecular weight, theoretical isoelectric point, atomic composition, and stability index were predicted by the ProtParam tool of online ExPASy https://web.expasy.org/protparam/). The secondary structure of PSCK-S was predicted according to PRABI GERLAND (https://npsa-prabi.ibcp.fr/NPSA/npsa_sopma.html). TMHMM (http://www.cbs.dtu.dk/services/TMHMM/) predicts the transmembrane structure of PSCK-S. ExPASy ProtScale tool (https://web.expasy.org/protscale/) predicts the hydrophobicity of the PSCK-S amino acid sequence.

2.4. Computational docking simulations and molecular dynamics (MD)

The crystallographic protein structures for PSCK isozymes have not yet been elucidated. Therefore we constructed the 3D structures by homology modeling according to previous reports [15,16,20,21]. Each PSCK-B, PSCK-M, and PSCK-S protein structure was modeled using homology templates HHsearch [22] to find template proteins, and the 9 or 10 best template sequences were aligned by application of T-Coffee [23] in its fast mode. CHARMM [24] was used to perform all calculations and the lowest energy structure was selected. Pseudo-quadratic restraints with simulated annealing (PQR-SA) [25] augmented with statistical torsion angle potential [26] was used to shape and to generate PSCK isozymes' structures. Docking simulations were performed with two ligands, glycine and proline, using Autodock-Vina (http://vina.scripps.edu). MD simulations were conducted by performing 10 ns simulations in the presence of ADP using CHARMM. The initial structure for the simulation was generated using CHARMM-GUI [27] for PSCK isozymes and the solvation effect was considered by application of a generalized Born model with a simple switch function (GBSW) [28]. In every 1 ps for trajectory analysis, the structures were saved and the structural details including identification of the neighboring residues from ADP were measured after a 10 ns production.

2.5. Determination of biochemical enzyme activities

Different tissues were quickly isolated and homogenized in PBS (0.01 M) using a homogenizer in an ice-bath. The supernatant was obtained by freezing centrifugation at 5000 rpm for 15 min for biochemical parameters' assay. The total activity of PSCK from the tissues was measured following proton generation during the reaction of ATP and creatine with thymol blue at 597 nm and 25 °C, as previously described [15,16,29,30]. The activities of total superoxide dismutase (T-SOD), lactate dehydrogenase assay (LDH), malondialdehyde (MDA), catalase (CAT), and the content of ATP were measured according to the kit

manuals (A020-2 for LDH, A001-1 for T-SOD, A007-1 for CAT, A003-2 for MDA, and A095 for ATP) provided by Nanjing Jiancheng Biochemical Reagent Co. Ltd. (Nanjing, China) using the clinical biochemical indicator autoanalyzer: Infinite M200Pro spectrometer (Tecan, Switzerland), according to the manufacturer's instructions.

2.6. Detection of PSCK isozymes' expression at the transcriptional level

The total RNA was extracted from these frozen tissues using the Trizol reagent (Invitrogen) according to the manufacturer's instructions, used for first-strand DNA synthesis reagent kit (Takara Bio Inc., Dalian, China). Real-time quantitative PCR was performed using the standard SYBR Green PCR kit (Takara Bio Inc.) and an ABI 7500 Thermocycler Real-Time PCR instrument (Applied Biosystems, Foster City, CA, USA). Gene expression was assessed using the $^{\Delta\Delta}C_t$ method. All qRT-PCRs analyses were performed in triplicate and the data are presented as means ± standard errors of the means (SEM). The primers used are as follows: β-actin, 5′- CCCAT ACTGT GCCCA TCTAC GA -3 (forward) and 5′- CCTCT GGACA CCTGA ACCTC TC -3′ (reverse); CK-B, 5′- GGACC CCAAC TATGT ACTAA GCTC -3′ (forward) and 5′- CCAGT CCCGT GCCAT TCCAG A -3′ (reverse); CK-M 5′- TGCTC ACCTG CCCGT CCAAC CT -3 (forward) and 5′- CTTCA CGCCG TCCAC CACCA TC -3′ (reverse); CK-S, 5′- GACCT CCGCA AACAT AACAA CT -3′ (forward) and 5′- GACTC TTCAT CACCA GCAAC CA -3′ (reverse).

2.7. Western blot analysis of PSCK isozymes

Tissues were homogenized in an ice-cold RIPA buffer containing 0.1% phenylmethylsulfonyl fluoride. The dissolved proteins were collected from the supernatant after centrifugation at 12,000 ×*g* for 20 min. Protein concentrations were determined using Coomassie blue-based assay reagent and then quantified. Protein extracts were separated by SDS-polyacrylamide gel electrophoresis and then electro-transferred onto a polyvinylidene difluoride (PVDF) membrane. The membrane was blocked with 5% BSA and then incubated at 4 °C overnight with respective primary antibodies for anti-CK-B antibody (ab151579, Abcam, USA; 1:1000 in PBST), anti-CK-M antibody (ab151465, Abcam, USA; 1:1000 in PBST), anti-CK-S antibody (ab189314, Abcam, USA; 1:800 in PBST), and anti-β-actin (inner control, ab8227, Abcam, USA; 1:1500 in PBST). After washing with Tris-buffered saline Tween-20 (TBST), the membranes were incubated with a goat anti-rabbit secondary antibody conjugated to HRP for 1 h at room temperature. The antibody reactive bands were visualized using enhanced chemiluminescence detection reagents and a gel imaging system (Tanon Science & Technology Co., Ltd., China).

2.8. Immunohistochemistry of PSCK isozymes

The tissues were fixed overnight in a 10% formaldehyde solution (dissolved in phosphate buffer, pH 7.4) and then embedded in paraffin as a standard histological method. Sections (6 μm, Leica RM 2125, Germany) were de-paraffinized and hydrated before staining. The sections were incubated in 3% H_2O_2 for 10 min to block endogenous peroxidase activity. The sections were then heated in a microwave oven for antigen retrieval in 0.01 M citrate for 10 min. The slides were subsequently blocked in 1% BSA and incubated with a primary antibody CK-B (1:100), CK-M (1:100) and CK-S (1:100) at 4 °C overnight. After rinsing with 0.01 M PBS, the sections were incubated with Rabbit IgG SABC Kit (Boster, Wuhan, China, SA1022). Following a second rinsing with 0.01 M PBS, the reaction products were visualized by the addition of chromogenic substrate 0.1% diaminobenzidine solution (Sigma-Aldrich, St. Louis, MO, USA) in 0.1% hydrogen peroxide in PBS and incubated for 5 min. Subsequently the slides were lightly counterstained with Harris hematoxylin. Finally, the slides were examined by light microscopy (Nikon 80i, Tokyo, Japan). Negative controls were performed with diluent normal rabbit serum (1:500) instead of the primary antibody.

2.9. Statistical analysis

Statistical analysis was performed by a one-way analysis of variance (ANOVA), and its significance assessed by Tukey's test. Data were presented as mean ± standard deviation (SD) and a value of $p < 0.05$ was considered statistically significant.

3. Results

3.1. Sequence and structure analysis of PSCK-S

The sizes of PCR products of Primer 1 and 2 were 774 bp and 662 bp respectively, as expected by monoclonal sequencing. Containing the whole CDS area of PSCK-S, the obtained sequence was 1352 bp by splicing, encoding a total of 419 amino acids as shown in Supplementary Data Supplementary Data 1.

The bioinformatics analysis is as follows: the molecular weight of PSCK-S is 47.35 kDa; the isoelectric point is 8.62; the molecular formula is $C_{2096}H_{3324}N_{598}O_{615}S_{19}$; the total number of negatively charged residues (ASP + Glu) is 54; the total number of positively charged residues (Arg + Lys) is 59; the N-terminal of the sequence is M (MET), and the instability index is 35.02 (>40 is unstable protein), indicating that PSCK-S protein is a stable protein. The probability of signal peptide cleavage site was predicted as 0.0537 (<0.45), indicating that PSCK-S has no signal peptide. According to the ProtScale tool's hydrophobicity analysis using ExPASy, the minimum value is −2.956, located at 42; the maximum value is 2.522, located at 195, and the average coefficient of hydrophilicity (GRAVY) is −0.443, suggesting that PSCK-S is a hydrophilic protein. The secondary structure of PSCK-S was predicted. The results showed that the irregular curl accounted for 40.81%, α-helix for 37.95%, β-sheet for 6.92%, and elongation chain for 14.32%. The results of domain prediction show that PSCK-S has ADP binding site, creatine binding site and substrate specific ring, which belongs to the creatine phosphokinase superfamily. The other two isozymes (PSCK-B and PSCK-M) were also analyzed and the data are displayed in Supplementary Table 2. Based on the secondary structure, both PSCK-B and PSCK-M have a high structural similarity while PSCK-S displays a unique structure compared to PSCK-B and PSCK-M as shown in Supplementary Table 2.

For phylogenetic analysis of the CK-S gene, 145 amino acid sequences of CK-S (type II mitochondrial CK) by BLASTP search were selected, and the accession numbers were listed as Supplementary Data 2. Based on this result, a phylogenetic tree was constructed by a proximity method using MEGA software as shown in Fig. 1.

It was found that turtles have the closest relationship with the Chinese soft-shelled turtle (*P. sinensis*), followed by the same order Reptilia: Crocodilia, such as the Chinese alligator (*Alligator sinensis*), Indian alligator (*Gavialis gangeticus*), estuarine crocodile (*Crocodylus porosus*), and American alligator (*Alligator mississippiensis*). These are followed by the central bearded dragon (*Pogona vitticeps*), green lizard (*Anolis carolinensis*), and gecko (*Gekko japonicus*). However, birds, platypus (*Ornithorhynchus anatinus*), and opossum (*Monodelphis domestica*), *etc.* of different orders of *P. sinensis* are only distantly related.

Next, the comparison of amino acid sequence for subtypes of PSCK was conducted. By comparing the amino acid sequences of three existing subtypes of PSCK, we found that PSCK-S had 418 amino acid codes, while the other two subtypes were 381 amino acids (Fig. 2). PSCK-S had a longer C-terminal and N-terminal. Through sequence comparison, the similarity between PSCK-S and PSCK-B is 56.9%, and the similarity between PSCK-S and PSCK-M is 59.29%. It is indicative that PSCK-B and PSCK-M have a high structural similarity in comparison with PSCK-S, which could connect to functional roles in physiological conditions. PSCK-S might additionally play a unique role *in vivo* beyond the simple function of creatine/phosphocreatine coupled ATP/ADP metabolic conversions, although this is not yet understood. Therefore, to reveal the new structure connected function and to make a comparison

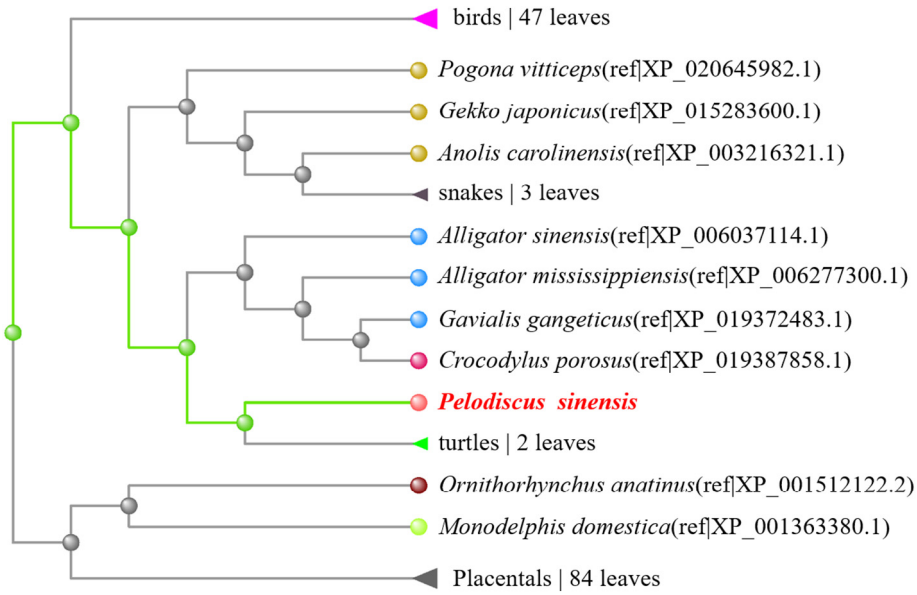

Fig. 1. Phylogenetic analysis of the PSCK-S amino acids sequence. Sequences were searched in NCBI database and selected by the parameters (Query cover = 100%; E value = 0; and Identities >85%), and the NJ (Neighbor Joining) tree was created by BLAST program.

between three subtypes of PSCKs, we conducted molecular docking simulations.

3.2. Computational homology modeling, docking simulations, and molecular dynamics of PSCK isozymes

We firstly established the 3D structure of PSCK-B, PSCK-M and PSCK-S and subsequently conducted the docking simulations and molecular dynamics (MD) between the substrate and each target enzyme. Based on the previous methods, we conducted homology modeling to construct each PSCK isozyme. In a sequence alignment shown in Supplementary Table 3, we found that a potent maximum sequence identity from a template combination is 0.95538 (best blosum = 0.92609 (1qh4_a); best seq. ID = 0.91601 (1qh4_a); best sum = 0.92105 (1qh4_a)) for PSCK-B. The potent maximum sequence identity from a template combination is 0.89501 (best blosum = 0.83532 (1qh4_a); best seq. ID = 0.81102 (1qh4_a); best sum = 0.82317 (1qh4_a)) for PSCK-M. The potent maximum sequence identity from a template combination is 0.73270 (best blosum = 0.58925 (1qh4_a); best seq. ID = 0.58711 (1qh4_a); best sum = 0.58818 (1qh4_a)) for PSCK-S. The alignment results are displayed in Supplementary Fig. 1. As a result, we found that the 3D structures between PSCK-B and PSCK-M had a strong similarity while the 3D structure of PSCK-S was slightly different from PSCK-B and PSCK-M (Fig. 3A). This had been intuitively expected from the sequence alignment analysis shown in Fig. 2. Next, we conducted computational docking simulations between PSCK isozymes and ADP (Fig. 3B). The active sites of binding pocket volumes were measured to give approximately 3062 $Å^3$ for PSCK-B; 2750 $Å^3$ for PSCK-M, and 2976 $Å^3$ for PSCK-S as shown. PSCK-B pocket volume was the largest and PSCK-M pocket volume the smallest. However, from the simple docking simulation we were hardly able to differentiate the distinctions of three isozymes. Moreover, by the application of the contact map as shown in Fig. 3C, we found no significant difference between the three contact maps where PSCK isozymes have the same tertiary structures and well-conserved active site regions. The measurement on similarity of their structures is not competent because of different residue numbers and in this situation, the contact map is useful since it represents how close three structures are by examining the pattern of maps. Fig. 3C showed the similar patterns of three contact maps, indicating three PSCK isozymes have the same fold of structure.

To gain more insight into the functional distinction between PSCK isozymes, we subsequently used analysis MD simulations (Fig. 4), which show the 10 ns dynamic change after ADP binding to each PSCK isozyme. As a result, we were interested to find that the exposed surface area of ADP binding sites for each isozyme displayed different data (Fig. 4A). After 10 ns MD simulations, exposed surface areas to ADP binding sites were changed: PSCK-S had a conspicuous change compared to PSCK-B and PSCK-M. Since PSCK-S has a larger surface area, we predict PSCK-S to have the strongest kinase activity. Furthermore, the analysis of gyration radius, commonly used as an indicator of protein structure compactness, showed PSCK-S to be a well-folded structure compared to the other two isozymes, with PSCK-B and PSCK-M displaying relatively over-compacted structures (Fig. 4B). The MD simulations indicated that PSCK-S as a mitochondrial form might have a high energy metabolic ratio and efficiency compared to the cytosolic forms of PSCK-B and PSCK-M, and intuited why PSCK-S is located in a mitochondrial site, the place of energy producing factory in animal cells. The overall data of computational 10 ns MD simulations between PSCK isozymes and ADP are listed in Table 1.

3.3. Determination of enzymatic and biochemical parameters in response to immunologic challenge

In order to detect the functional distinction of PSCK in *P. sinensis*, the influence of bacterial infection on total PSCK activity change during the immune response was measured. Simultaneously, several immunological factors including MDA and ATP contents, the activities of TSOD (total SOD), CAT and LDH were examined in *P. sinensis* tissues such as the myocardium, liver, spleen, kidney and skeletal muscle (Fig. 5). The results show that the total PSCK activity was significantly reduced in the myocardium and skeletal muscle after bacterial infection, slightly decreased in the liver and kidney (no statistical significance), and significantly increased in the spleen (Fig. 5A). The MDA content was significantly decreased in all examined tissues (Fig. 5B). TSOD activity was significantly increased in sample tissues except for the skeletal muscle sample (Fig. 5C). ATP content, which is directly associated with PSCK function, had mixed patterns: down-regulated in the myocardium and spleen, and up-regulated in the liver, kidney, and skeletal muscle (Fig. 5D). LDH activity was significantly decreased in the myocardium and spleen, increased in the liver and skeletal muscle, and

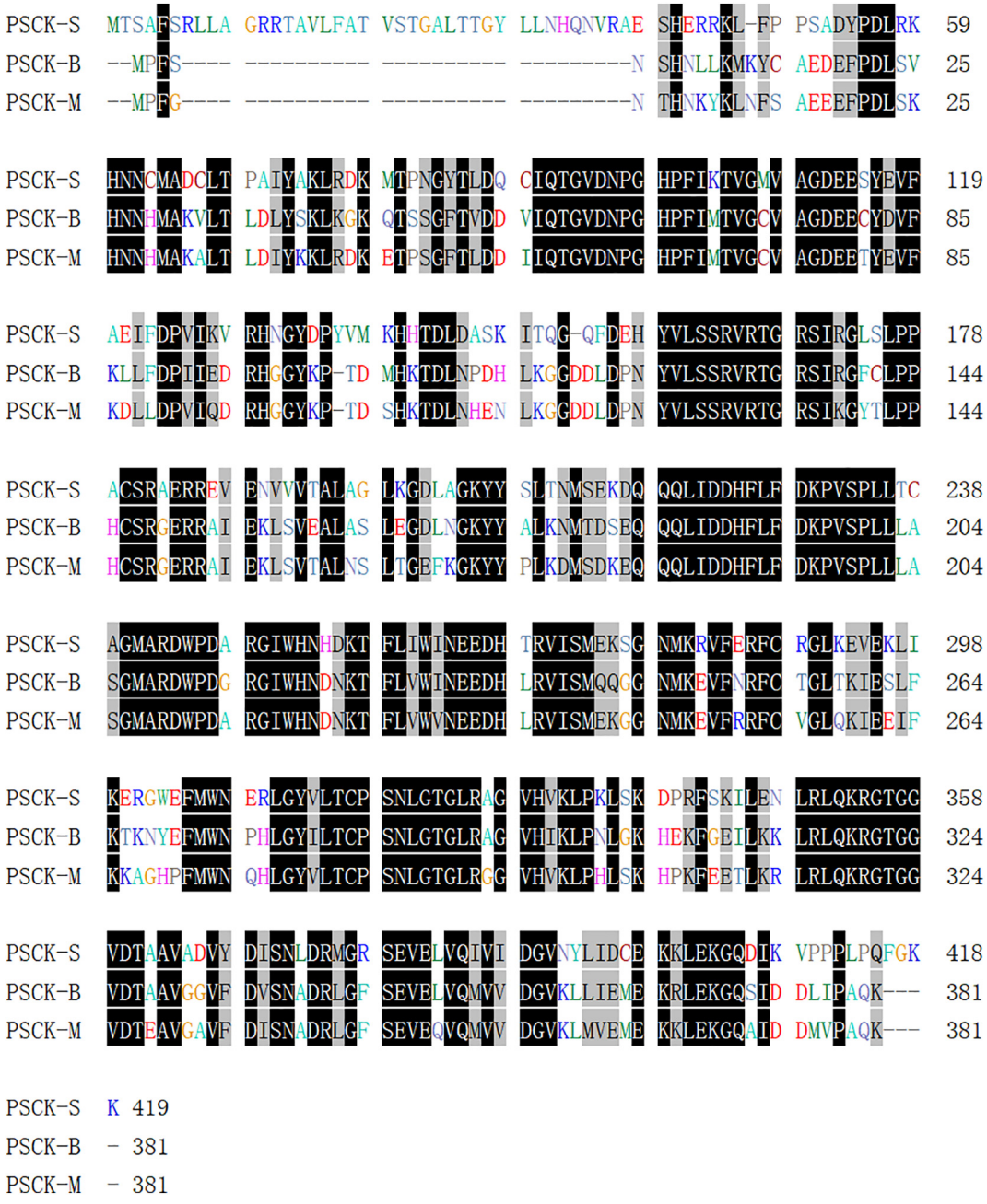

Fig. 2. Multiple sequence alignment of amino acids sequences for PSCK isozymes by a program Clustal W. Dark shaded characters represented the amino acids that were exactly the same in the alignment of the three sequences; Gray shaded characters represented the three amino acids are not identical in sequence alignment, but with the same polarity; The unshaded characters represented the three amino acids are not identical in sequence alignment, and of different polarity.

normal levels detected in the kidney (Fig. 5E). CAT activity was detected as significantly decreased in the myocardium, spleen, and kidney, significantly increased in skeletal muscle, and no statistically significant change in the liver (Fig. 5F). In general, the tissues most affected by bacterial infection in *P. sinensis* were the myocardium and spleen shown in the indexes displayed in Fig. 5 as significantly changed, followed by the muscle, kidney, and liver.

3.4. Real-time RT-PCR analyses of PSCK isozymes in various tissues

The expression levels of three kinds of PSCK isozymes were examined by real-time RT-PCR (Fig. 6). The results showed that the expression level of PSCK-B was significantly reduced in the myocardium, while significantly increased in the liver and spleen (Fig. 6A). For PSCK-M, the expression level was significantly reduced in the myocardium, while significantly increased in the liver (Fig. 6B). For PSCK-S, the expression level was significantly reduced in the myocardium and skeletal muscle, while significantly increased in the spleen (Fig. 6C). In addition, a stack histogram was plotted for gene expression in different tissues (Fig. 6D). The results show that PSCK-B was predominantly expressed in liver and kidney (>60%), PSCK-M was predominantly expressed in the muscle (>60%), and PSCK-S was predominantly expressed in the spleen (>60%). In the myocardium, PSCK-S was the predominant type (42%), followed by PSCK-B and PSCK-M. These results indicate that PSCK isozymes genes apparently exhibit a tissue-specific expression, and that PSCK isozymes genes also show an inconstant expression pattern in a specific tissue after bacterial infection. The PSCK isozymes genes represent various expression levels and may take different functions in energy metabolism in response to immunological issues.

A

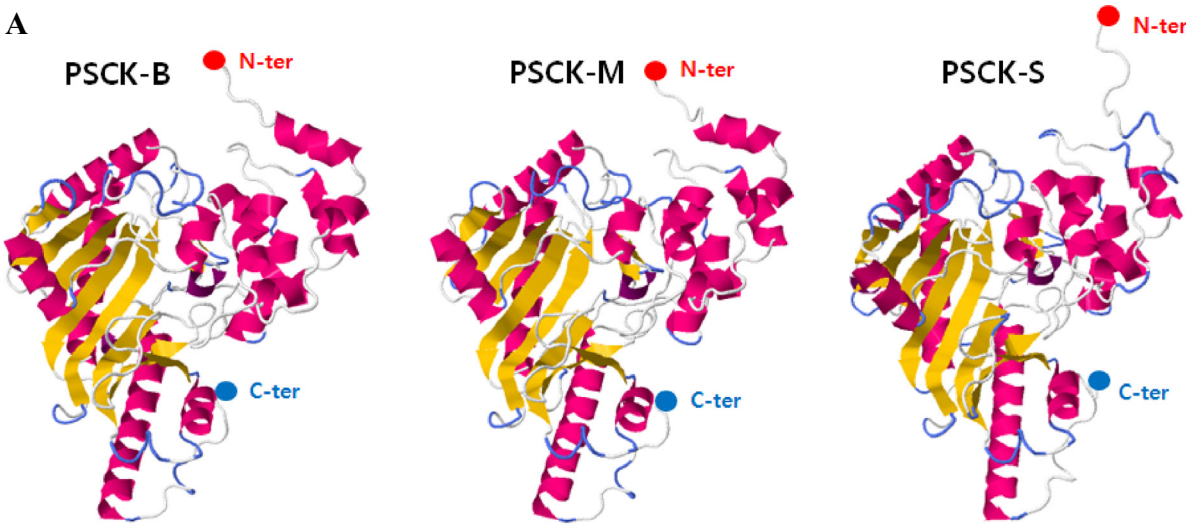

B

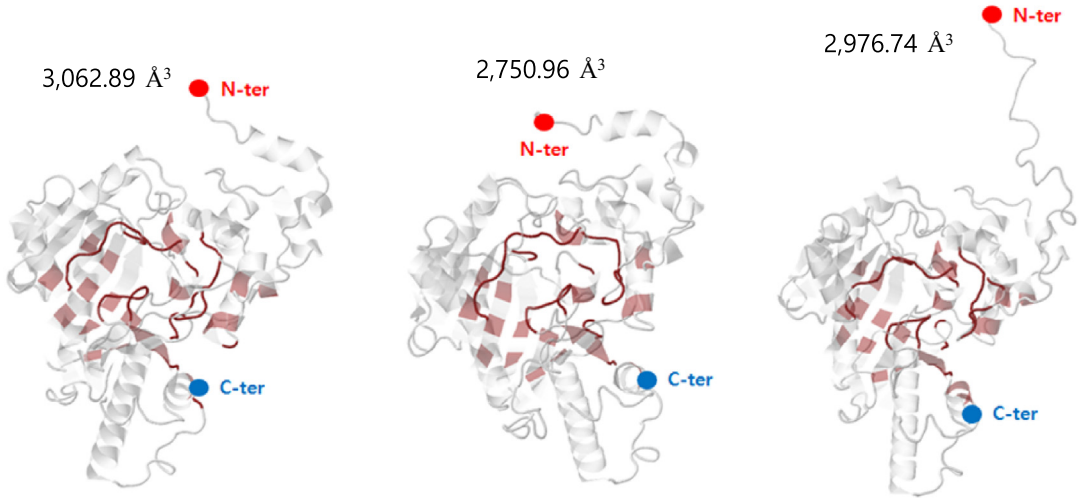

PSCK-B

HSD29 LYS32 HSD66 PHE68 ILE69 MET70 THR71 VAL72 GLY73 CYS74 VAL75 ASP95 ARG96 GLY98 ARG130 ARG132 ILE188 HSD191 PHE192 LEU193 PHE194 ASP195 LYS196 PRO197 VAL198 SER199 LEU201 LEU202 TRP228 GLU231 GLU232 ARG236 ILE238 MET240 CYS283 SER285 ASN286 ARG292 HSD296 LYS313 ARG316 LEU317 GLN318 ARG320 THR322 GLY323 GLY324 VAL325 ASP326 THR327 ASP335 ALA339 ASP340 ARG341 GLN380

PSCK-M

CYS63 ASP66 ASN97 GLY99 HSD100 ILE103 LYS104 THR105 VAL106 GLY107 MET108 VAL109 VAL129 ARG130 ARG164 ARG166 ILE222 HSD225 LEU227 PHE228 ASP229 LYS230 PRO231 VAL232 SER233 PRO234 LEU235 LEU236 TRP262 GLU265 GLU266 ARG270 ILE272 MET274 CYS317 SER319 ASN320 ARG326 HSD330 SER343 LEU346 GLU347 ARG350 LEU351 GLN352 LYS353 ARG354 THR356 GLY357 GLY358 VAL359 ASP360 THR361 ASP369 LEU373 ARG375

PSCK-S

HSD29 HSD66 PHE68 ILE69 MET70 THR71 VAL72 GLY73 CYS74 VAL75 ASP95 ARG96 ARG130 ARG132 ILE188 HSD191 PHE192 LEU193 PHE194 ASP195 LYS196 PRO197 VAL198 SER199 LEU201 LEU202 TRP228 GLU231 GLU232 ARG236 ILE238 MET240 CYS283 SER285 ASN286 ARG292 HSD296 LYS313 ARG316 LEU317 GLN318 ARG320 THR322 GLY323 GLY324 VAL325 ASP326 THR327 ASP335 ALA339 ASP340 ARG341

C

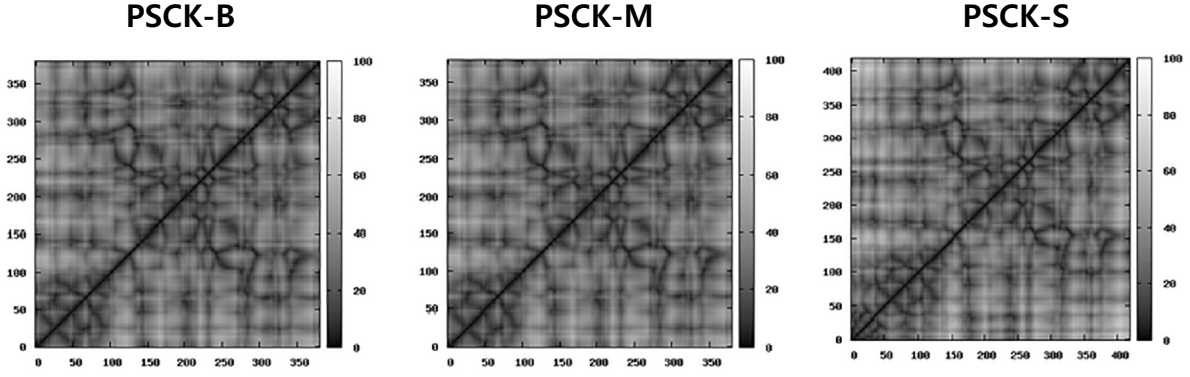

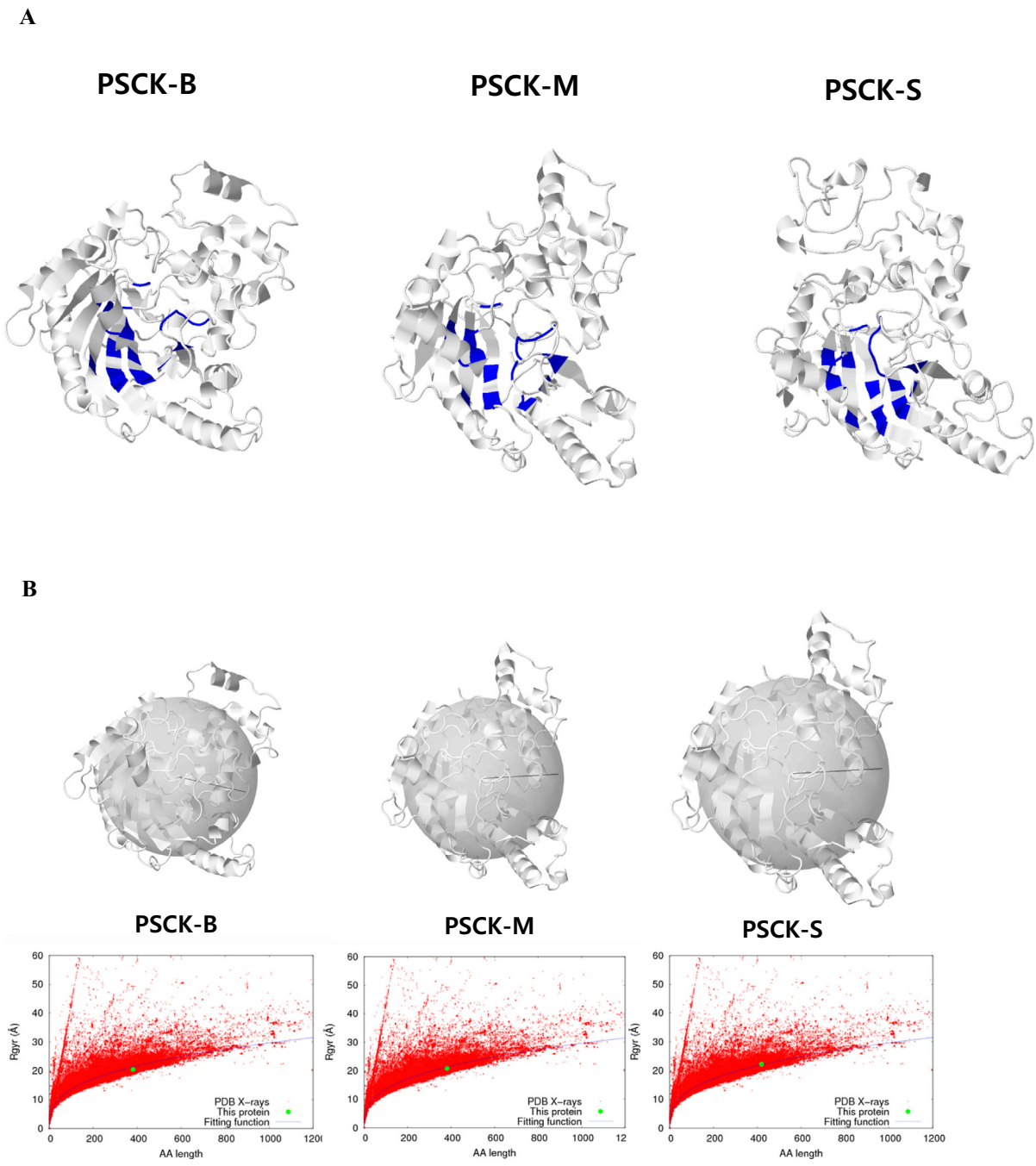

Fig. 4. 10 ns molecular dynamics (MD) simulations results. (A) Exposed surface area of ADP binding sites. After 10 ns MD simulations, exposed surface areas to ADP binding sites are labeled as blue colors where the ADP binding sites (blue colors) of three structures are kept after 10 ns MD simulation. (B) Radius of gyration. The radius of gyration is an indicator of protein structure compactness. A globular protein has larger radius of gyration as the protein sequence grows. The blue line in the below figure represent the fitting curve in whole high resolution X-ray structures deposited in Protein Data Bank (PDB). These results are the same concept of ADP binding site conservation in (A) on which their structures are well stable and kept the ADP binding site irrespective of MD simulations.

3.5. Western blot analysis of PSCK isozymes in various tissues

Alterations in PSCK isozymes expression in different tissues were also examined by the western blotting method (Fig. 7). For each type of isozymes (PSCK-B, PSCK-M, PSCK-S), control group (CG) and infection group (IG) were individually detected and the expression level was compared (Fig. 7A). The results demonstrate that after bacterial infection, the expression of PSCK-B was significantly increased in the myocardium, liver and spleen while there was no change in the kidney and skeletal muscle (Fig. 7B). For PSCK-M, the expression

Fig. 3. Computational docking simulation between PSCK isozymes and ADP. (A) Homology modeling structures of PSCK isozymes. The protein structures are drawn by cartoon image and colored by red (helix), yellow (sheet), and blue (coil). The N- and C-terminals are marked with red and blue spheres, respectively. (B) Plausible ADP binding site volumes and pocket residues. The structures are drawn by white cartoon image and the ADP binding sites are colored by red. The plausible ADP binding sites consisting of pocket residues are tabulated below the structure. (C) Contact maps for PSCK isozymes. The contact map is obtained by measuring the distance of two selected alpha Carbon atoms. The darker color indicates the closer distance between two residues. The X- and Y-axes represent the residue numbers of the structure. Three structures have different sequences and numbers of residues.

Table 1
Structural analysis after 10 ns MD simulations between PSCK isozymes and ADP.

Subject	PSCK-B	PSCK-M	PSCK-S
Number of total amino acids	381	381	419
% of exposed/buried residues	35/65	33/67	33/67
% of Secondary structure (H/E/C)[a]	35/15/50	35/13/52	32/13/55
Exposed surface area of ADP binding sites (Å^2)	74	155	272
Radius of gyration (Å)	20.47	20.79	22.20

[a] H/E/C: helix, sheet, random coil ratios.

level was significantly increased in the liver, decreased in the myocardium and skeletal muscle, and no change detected in the spleen and kidney (Fig. 7C). For PSCK-S, the expression level was significantly increased in the spleen, decreased in the myocardium and skeletal muscle, and no change detected in the liver and kidney (Fig. 7D). Using western blotting analysis, we observed that PSCK isozymes were specifically expressed in tissues and differentially regulated in response to immune stress by bacterial infection. When we compared the results of transcriptional level (real-time RT-PCR, Fig. 6) and translational level (western blotting, Fig. 7), we found consistency except for expressions of PSCK-B in the myocardium and PSCK-M in the skeletal muscle. The results of the comparison between real-time RT-PCR and western blot analysis are listed in Table 2. Taken together, our results suggest that the expression levels of PSCK isozymes were decreased overall in the myocardium and skeletal muscle, and increased in the liver and spleen. However, in the kidney bacterial infection had no effect on the expression level of PSCK isozymes.

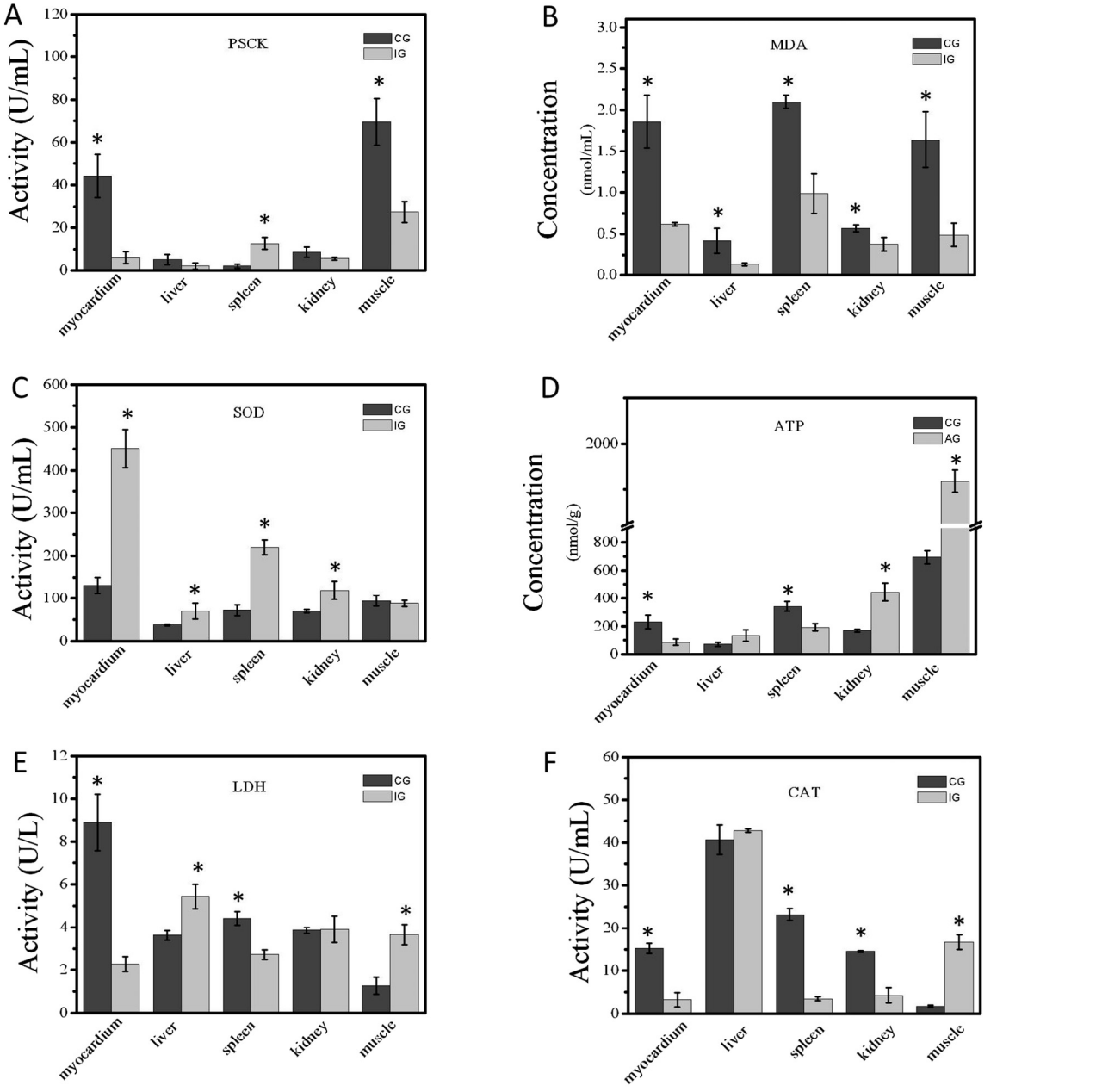

Fig. 5. Determination of biochemical parameters after bacterial infection. *, $p < 0.05$; CG, control group; IG, infection group; MDA, malondialdehyde; SOD, superoxide dismutase; ATP, adenosine triphosphate; LDH, lactate dehydrogenase; CAT, catalase. The total activity of PSCK from tissues were measured following proton generation during the reaction of ATP and creatine with thymol blue at 597 nm and 25 °C and the activities of total SOD, LDH, MDA, CAT, and the content of ATP were measured according to the kit manuals provided by Nanjing Jiancheng Biochemical Reagent Co. Ltd. (Nanjing, China) using a clinical biochemical indicator autoanalyzer Infinite M200Pro spectrometer (Tecan, Switzerland) according to the manufacturer's instructions. All analyses were performed in triplicate and the data are presented as means ± standard errors of the means (SEM).

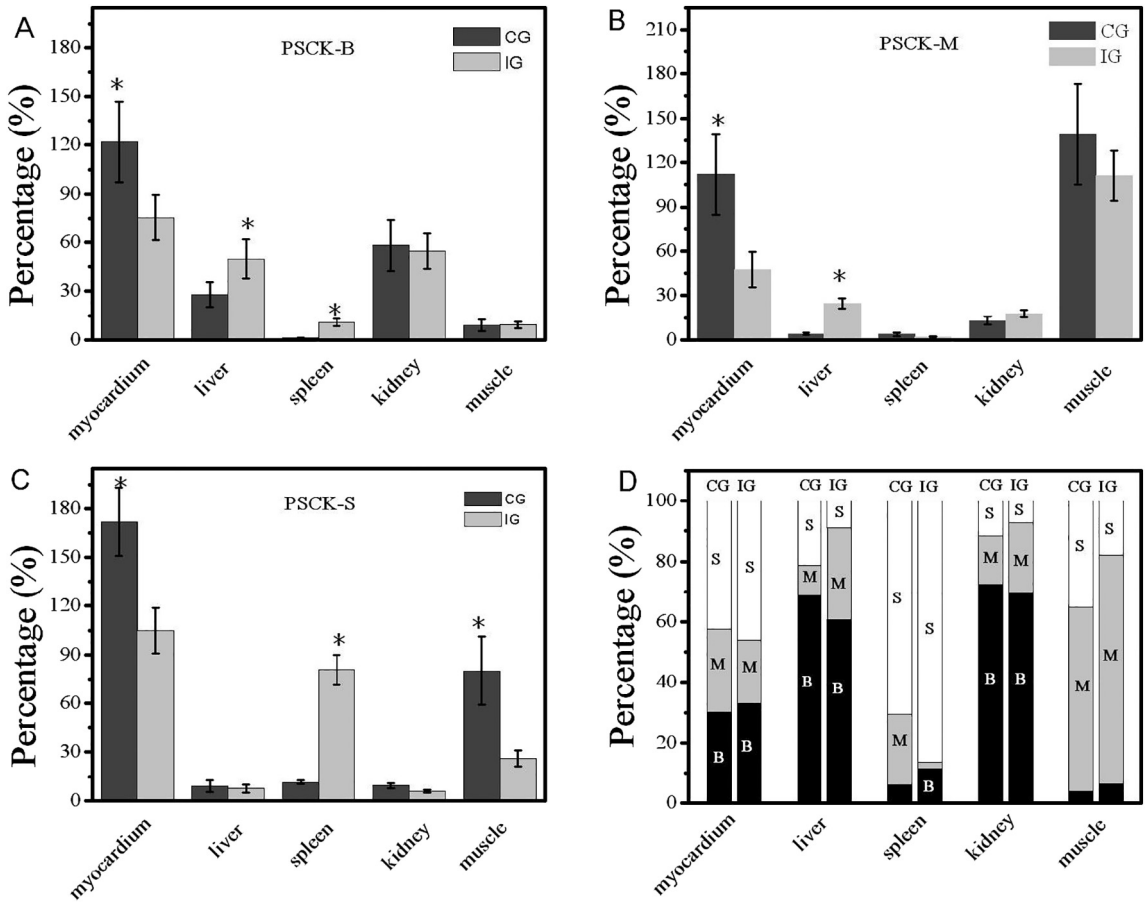

Fig. 6. Real-time RT-PCR analysis of PSCK isozymes expressions in different tissues after bacterial infection. (A) to (C), mRNA level expression of PSCK-B, PSCK-M and PSCK-S; (D) the ratio of mRNA expression for different PSCK isozymes in different tissues. *, $p < 0.05$; CG, control group; IG, infection group. Real-time quantitative PCR was performed using the standard SYBR Green PCR kit (Takara Bio Inc.) and an ABI 7500 Thermocycler Real-Time PCR instrument (Applied Biosystems, Foster City, CA, USA). Gene expression was assessed using the $^{\Delta\Delta}C_t$ method. All analyses were performed in triplicate and the data are presented as means ± standard errors of the means (SEM).

3.6. Immunohistochemistry (IHC) analysis of PSCK isozymes in various tissues

In the next step, we conducted the analysis of IHC to understand the expression of PSCK isozymes *in vivo* conditions. The IHC staining of PSCK isozymes in various *P. sinensis* tissues is displayed in Fig. 8. The results showed that three types of PSCK isozymes were widely expressed in myocardial fiber (MF) (Fig. 8A) and hepatocyte (Fig. 8B) before and after immunization. However, after immune stress (Fig. 8C), the expression of PSCK-B (Fig. 8C2) and PSCK-S (Fig. 8C6) were significantly increased in the spleen. The expression was mainly concentrated in the spleen nodule (SN) and the peripheral lymphatic sheath (PLS), and also detected in the central artery epithelial cells. The expression of PSCK-M (Fig. 8C3 and C4) in the spleen was weak before and after immune stress. The expression of PSCK-B (Fig. 8D2) and PSCK-M (Fig. 8D4) mostly decreased after immune stress in the kidney, but the expression and location of the three subtypes were significantly different. The three subtypes were highly expressed in the distal convoluted tubule (DCT), and slightly expressed in the proximal convoluted tubule (PCT) and glomerulus (G) (Fig. 8D). It should be noted that the expression of PSCK-S in glomerulus (G) increased after immune stress (Fig. 8D6). The expression localization of the three PSCK subtypes in the skeletal muscle was similar to that in the myocardium, and abundantly expressed in muscle fiber (SMF) (Fig. 8E). However, the expression of PSCK-S changed slightly after immune stress (Fig. 8E6).

In cases of immune emergency, the spleen is an important immune organ. PSCK-B and PSCK-S exhibited the strongest signals in the spleen following bacterial infection, consistent with the results in Table 2.

4. Discussion

It is generally recognized that high energy costs would be required in a defensive mechanism against a bacterial infection or various disease associated physiological conditions [31–35] where CK-mediated metabolisms were thought to be important. The regulation of CK is directly linked to energy balance, energy producing systems, and energy metabolites (creatine/phosphocreatine, ATP/ADP) demanded in the various pathogenesis. In the present study, an energy demanding situation was designed as a bacterial infection to produce immunologic stress in *P. sinensis*. Serial tests were conducted to find alterations of PSCK isozymes' expression during immune response, including several basic metabolic parameters such as MDA, ATP, TSOD, LDH, and CAT.

Previous reports have discussed the biochemical characteristics of PSCK in *P. sinensis*, mainly focusing on the muscle (PSCK-M) and brain (PSCK-B) types *in vitro* folding studies [15,16,20,21,29,30]. In this study, we have focused on the mitochondrial type such as PSCK-S and made a comparison between three types of PSCK isozymes. We have also completed serial studies coupled with *in vitro* and *in vivo* conditions to reveal the PSCK isozymes' expression and their putative functional roles associated with bacterial infection induced immunologic stress in *P. sinensis*. In the first part, we analyzed and compared the PSCK

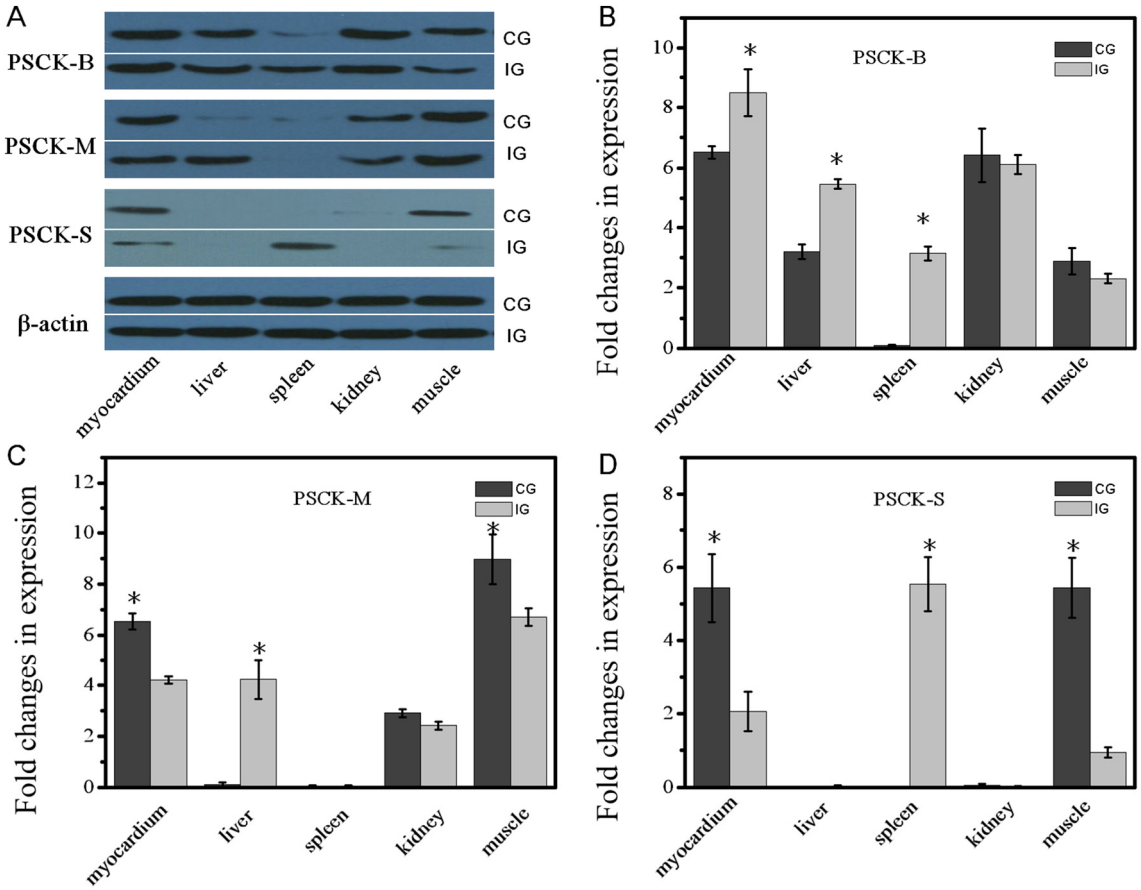

Fig. 7. Western blot analysis of PSCK isozymes expressed in different tissues after bacterial infection. (A) the immunoblotting results of PSCK isozymes; (B) to (D) comparison of protein expression levels of PSCK-B, PSCK-M and PSCK-S after bacterial infection; *, $p < 0.05$; CG, control group; IG, infection group. The primary antibodies were for anti-CK-B antibody (ab151579, Abcam, USA; 1:1000 in PBST), anti-CK-M antibody (ab151465, Abcam, USA; 1:1000 in PBST), anti-CK-S antibody (ab189314, Abcam, USA; 1:800 in PBST), anti-GAPDH (inner control, ab181602, Abcam, USA; 1:1500 in PBST).

isozymes using bioinformatic tools including computational docking and MD simulations. The results indicated that PSCK-S has a unique response to ADP in comparison with PSCK-B and PSCK-M, that supports the location of PSCK-S in mitochondria as a type II isoform and might play a role in energy fluctuation. In a 10 ns dynamic based MD simulation, we were interested to find that PSCK-S had a conspicuous change of exposed surface area to ADP binding sites, and a larger surface area than predicted by PSCK-B and PSCK-M, implying that PSCK-S has a relatively stronger kinase activity. In addition, the radius of gyration analysis indicated that PSCK-S has a well-folded structure to conduct proper catalytic functions.

In the second part, we checked the total PSCK activity with several metabolic parameters. We induced immunologic stress in *P. sinensis* through bacterial infection and different samples were collected from *P. sinensis* tissues to understand the physiological changes. In response to the bacterial infection, systemic changes in various tissues were observed:

(i). PSCK showed mixed patterns: the decrease of ATP content in the spleen and the up-regulation of PSCK activity in the spleen indicated the occurrence of high energy consuming mechanisms, while down-regulation of PSCK activity directly resulted in an increase of ATP content in the liver, kidney, and skeletal muscle.

(ii). The concentration of MDA was significantly reduced in all examined tissues, indicating an anti-fatigue function or anti-oxidative stress mechanism in *P. sinensis* was well developed under the condition of bacterial-induced immune stress. Since MDA is an indicator of oxidative stress, lipid peroxidation and an aggravator of oxidative damage, and is directly associated with the regulation level of antioxidant enzymes such as TSOD and CAT which play a pivotal role in the detoxification of reactive oxygen species (ROS)-mediated oxidative stress; the low concentration of MDA is directly connected with the results of up-regulated activity of TSOD in overall tissues.

(iii). Interestingly, TSOD was not up-regulated in skeletal muscle, and CAT was detected as only up-regulated in skeletal muscle and down-regulated other tissues, implying a compensation manner among these two antioxidant enzymes for restoring energy efficiency and avoiding redundant bi-expression during immune response in *P. sinensis*. Also, the content of free radicals and peroxidation of membrane lipids, accompanied with the high level of TSOD or CAT activity and low level of MDA content, are thought to be reduced because the increased activity of TSOD

Table 2
Comparison between real-time RT-PCR (qPCR), western blot (WB), and immunohistochemistry (IHC) analyses under immune stress.

Tissues	PSCK-B			PSCK-M			PSCK-S		
	qPCR	WB	IHC[a]	qPCR	WB	IHC[a]	qPCR	WB	IHC[a]
Myocardium	−	+	□	−	−	△	−	−	△
Liver	+	+	□	+	+	○	/	/	△
Spleen	+	+	○	/	/	△	+	+	○
Kidney	/	/	△	/	/	△	/	/	□
Skeletal muscle	/	/	△	/	−	△	−	−	○

(+) indicates the expression level significantly increased; (−) indicates the expression level significantly decreased; (/) indicates no change with significance.

[a] Signal intensity comparative to control: (○) strong; (□) medium; (△) low.

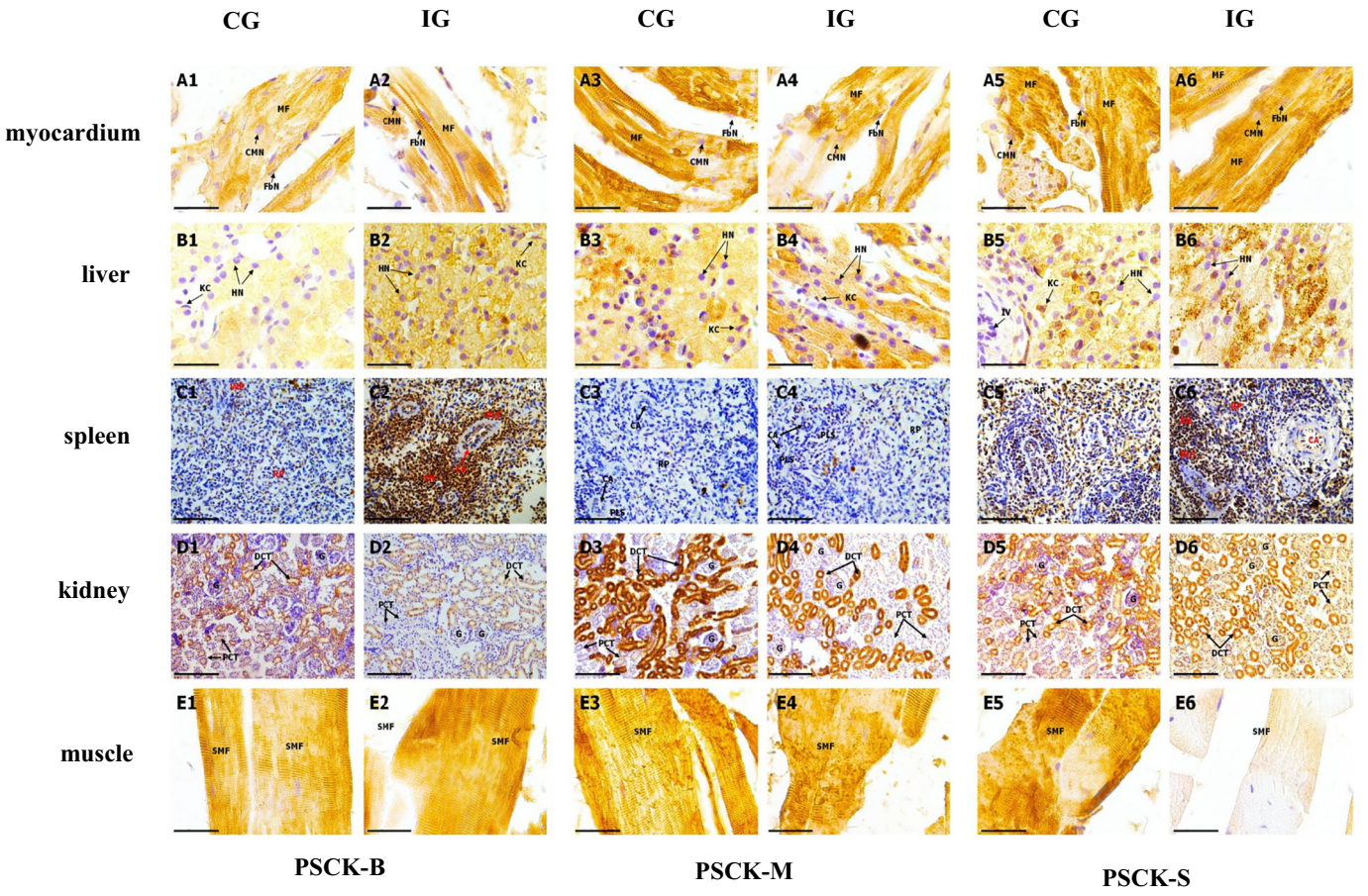

Fig. 8. Immunohistochemistry (IHC) staining of PSCK isozymes in various tissues after bacterial infection. The size bars indicate 30 μm for A, B and E; 150 μm for C and D. CMN, cardiac myocytes nuclear; FbN, fibroblast nuclear; MF, Myocardial fiber; KC, Kupffer's cells; HN, Hepatocyte nuclear; RP, red pulp; WP, white pulp; CA, central artery; SN, splenic nodule; PLS; periarterial lymphatic sheath; PCT, proximal convoluted tubule; DCT, distal convoluted tubule; G, glomus; IV, interlobular veins; SMF, skeletal muscle fiber. The primary antibody was used as CK-B (1:100), CK-M (1:100) and CK-S (1:100). The sections were incubated with Rabbit IgG SABC Kit (Boster, Wuhan, China, SA1022). Reaction products were visualized by addition of chromogenic substrate 0.1% diaminobenzidine solution (Sigma-Aldrich, St. Louis, MO, USA) in 0.1% hydrogen peroxide in PBS and the slides counterstained with Harris hematoxylin lightly. The slides finally were examined by light microscopy (Nikon 80i, Tokyo, Japan). Negative controls were performed with diluent normal rabbit serum (1:500) instead of the primary antibody.

and CAT directly inhibited MDA contents.

(iv). LDH is a marker of anaerobic metabolism connected to CK metabolism; thus LDH and CK are indicators of muscle injury and fatigue. The decrease of LDH in the myocardium and spleen indicates these tissues are susceptible to oxygen deprivation. However, LDH was increased in the liver and skeletal muscle. These results show that LDH and PSCK are not matched to the known indicator function; they are differently regulated during immune response in *P. sinensis* and in this case, muscle damage and fatigue is not a main defensive mechanism against bacterial infection since PSCK activity was detected as significantly reduced in the myocardium and skeletal muscle. LDH is also an indicator of oxidative stress, therefore LDH is thought to be more prone to connect with oxidative stress exposure and is similar to TSOD and CAT expression.

In the third part, we performed real-time RT-PCR and western blotting analysis in various tissues of *P. sinensis*, and revealed that the expression levels of PSCK isozymes were decreased in the myocardium and skeletal muscle, increased in liver and spleen, and had no significant change in the kidney. Due to the activity assay being only applicable for the total PSCK enzyme, subtypes of PSCK isoforms could not be measured; however, expressions of transcriptional and translational levels could be separately detected. Interestingly, in skeletal muscle PSCK-S was down-regulated along with an increase in ATP content, implying that ATP is required for defensive mechanisms against bacterial infection as an important energy source. Thus, ATP restoration and storing might be obtained from down-regulation of PSCK-S, the isozyme possessing a powerful kinase function in its structure as shown in MD simulation. We intuit that the up-regulation of PSCK isozymes is connected to ATP usage while down-regulation is linked to ATP storing, and the energy fluctuation is somehow associated with the immune response in a different manner in *P. sinensis*. It is similarly indicative that various subtypes of CK in humans are detected as different expression levels, either up- or down-regulated in CK-related human diseases.

We also found that PSCK-B was down-regulated in the transcriptional level while it was over-expressed in the protein level (Table 2). This discrepancy is not clear, however, based on the data detected in this study, we hypothesized that due to the reason of "compensation effect", PSCK-B is to be up-regulated in the translational level to play a role of functional compensation for blocking the energetic imbalance in myocardium in response to bacterial infection. Sine other two subtypes of PSCKs (PSCK-M and PSCK-S) are simultaneously down-regulated both in transcriptional and translation levels, at least, the protein expression signal of PSCK-B should be drastically and specifically turned on in myocardium. The detailed signal and its associated factors for turning on the expression of PSCK-B could be an interesting topic in the further study.

Our results showed that different tissues responded in different ways against bacterial infection. The energy metabolism caused by PSCK isozymes and ATP did not occur in the kidney while at least one

of PSCK isozymes actively participated in an energy metabolism related defensive mechanism in the myocardium, liver, spleen, and skeletal muscle in different ways.

Finally, we conducted IHC staining in different tissues of *P. sinensis*. Coupled with the *in vitro* results, IHC staining *in vivo* samples provided informative data for each PSCK isozymes' expression. We found that PSCK-B exhibited the strongest signals in the spleen and PSCK-M exhibited the strongest signals in the liver. PSCK-S exhibited the strongest signals in the spleen and a conspicuous alteration in skeletal muscle after bacterial infection, which is consistent with *in vitro* measurements of gene/protein expression levels.

In summary, we compared three types of PSCK isozymes *via* computational simulations and expression detections *in vitro* and *in vivo*. As a result, we found that PSCK-S as predicted mostly possessed kinase function in a structural aspect, and PSCK isozymes are expressed differently in *P. sinensis* tissues in various ways under bacterial infection-induced immunologic stress. PSCK-S contributes to the spleen and is uniquely expressed in skeletal muscle, PSCK-B mostly contributes to the spleen, followed by the liver and myocardium, and PSCK-M mostly contributes to the liver, followed by the myocardium and skeletal muscle. These various alterations of PSCK isozymes in tissues are prone to defense the bacterial infection and blocking energetic imbalance before severe pathogenesis turned on in *P. sinensis*. Our results suggest that the regulation of PSCK played an important function in the energy metabolism of *P. sinensis* under an immune stress challenge, and it could enlarge the area of the energy-related function of CK in other reptiles.

Supplementary data to this article can be found online at https://doi.org/10.1016/j.ijbiomac.2020.06.036.

Author statement

Caiyan Li: Conceptualization, Methodology, Software, Data curation.
Wei Wang: Conceptualization, Methodology, Software.
Jinhyuk Lee: Visualization, Investigation, Data curation.
Lifang Zeng: Visualization, Investigation, Data curation.
Yufei Yang: Software, Validation, Data curation.
Shang-Jun Yin: Supervision, Writing - Reviewing and Editing.
Yong-Doo Park: Supervision, Writing - Original draft preparation and Editing.
Guo-Ying Qian: Supervision, Writing - Reviewing and Editing.

Declaration of competing interest

None.

Acknowledgements

This research was supported by the Major Agricultural Project of Ningbo (2017C110012) and the Zhejiang Provincial Project of Selective Breeding of Aquatic New Varieties (2016C02055-4-4). Dr. Caiyan Li was supported by the grants from National Natural Science Foundation of China (31802272) and Zhejiang Provincial Natural Science Foundation (LY18C190001). Dr. Wei Wang was supported by National Natural Science Foundation of China (31402278) and the Top Key Discipline of Bioengineering in Zhejiang Province (ZS2018006). Dr. Yong-Doo Park was supported by a fund from the Public Project of Jiaxing City (2018AY32042).

References

[1] T. Wallimann, M. Wyss, D. Brdiczka, K. Nicolay, H.M. Eppenberger, Intracellular compartmentation, structure and function of creatine kinase isoenzymes in tissues with high and fluctuating energy demands: the 'phosphocreatine circuit' for cellular energy homeostasis, Biochem. J. 281 (1992) 21–40, https://doi.org/10.1042/bj2810021.
[2] C.D. Cabaniss, Creatine kinase. In: H.K. Walker, W.D. Hall, J.W. Hurst, Clinical Methods: The History, Physical, and Laboratory Examinations (3rd edition), Boston, 1990. pp. 161–163.
[3] R. Guzun, N. Timohhina, K. Tepp, M. Gonzalez-Granillo, I. Shevchuk, V. Chekulayev, A.V. Kuznetsov, T. Kaambre, V.A. Saks, Systems bioenergetics of creatine kinase networks: physiological roles of creatine and phosphocreatine in regulation of cardiac cell function, Amino Acids 40 (2011) 1333–1348, https://doi.org/10.1007/s00726-011-0854-x.
[4] U. Schlattner, M. Tokarska-Schlattner, T. Wallimann, Mitochondrial creatine kinase in human health and disease, Biochim. Biophys. Acta 1762 (2006) 164–180, https://doi.org/10.1016/j.bbadis.2005.09.004.
[5] U. Schlattner, L. Kay, M. Tokarska-Schlattner, Mitochondrial proteolipid complexes of creatine kinase, Subcell. Biochem. 87 (2018) 365–408, https://doi.org/10.1007/978-981-10-7757-9_13.
[6] T. Wallimann, M. Tokarska-Schlattner, U. Schlattner, The creatine kinase system and pleiotropic effects of creatine, Amino Acids 40 (2011) 1271–1296, https://doi.org/10.1007/s00726-011-0877-3.
[7] K. Sahlin, R.C. Harris, The creatine kinase reaction: a simple reaction with functional complexity, Amino Acids 40 (2011) 1363–1367, https://doi.org/10.1007/s00726-011-0856-8.
[8] L. Owen, S.I. Sunram-Lea, Metabolic agents that enhance ATP can improve cognitive functioning: a review of the evidence for glucose, oxygen, pyruvate, creatine, and L-carnitine, Nutrients 3 (2011) 735–755, https://doi.org/10.3390/nu3080735.
[9] L. Qin, D. Dang, X. Wang, R. Zhang, H. Feng, J. Ren, S. Chen, G. Zhou, P. Huang, Y. Wang, W. Xi, Y. Wu, Jin, G. Duan, Identification of immune and metabolic predictors of severe hand-foot-mouth disease, PLoS One 14 (2019) e0216993, https://doi.org/10.1371/journal.pone.0216993.
[10] A. Flahault, M. Metzger, J.F. Chassé, J.P. Haymann, J.J. Boffa, M. Flamant, F. Vrtovsnik, P. Houillier, B. Stengel, E. Thervet, N. Pallet, Low serum creatine kinase level predicts mortality in patients with a chronic kidney disease, PLoS One 11 (2016), e0156433. https://doi.org/10.1371/journal.pone.0156433.
[11] J. Xu, X. Fu, M. Pan, X. Zhou, Z. Chen, D. Wang, X. Zhang, Q. Chen, Y. Li, X. Huang, G. Liu, J. Lu, Y. Liu, Y. Hu, S. Pan, Q. Wang, Q. Wang, Y. Xu, Mitochondrial creatine kinase is decreased in the serum of idiopathic Parkinson's disease patients, Aging Dis. 10 (2019) 601–610, https://doi.org/10.14336/AD.2018.0615.
[12] D.S. Hui, M.C. Chan, A.K. Wu, P.C. Ng, Severe acute respiratory syndrome (SARS): epidemiology and clinical features, Postgrad. Med. J. 80 (2004) 373–381, https://doi.org/10.1136/pgmj.2004.020263.
[13] F. Zheng, W. Tang, H. Li, Y.X. Huang, Y.L. Xie, Z.G. Zhou, Clinical characteristics of 161 cases of corona virus disease, 2019 (COVID-19) in Changsha, Eur. Rev. Med. Pharmacol. Sci. 24 (2020) 3404–3410, https://doi.org/10.26355/eurrev_202003_20711.
[14] S. Zheng, J. Wu, F. Yu, Y. Wang, L. Chen, D. Cui, G. Xie, X. Yang, X. Chen, W. Zhang, L. Yu, J. Guo, Y. Zhang, Y. Chen, Elevation of creatine kinase is linked to disease severity and predicts fatal outcomes in H7N9 infection, Clin. Chem. Lab. Med. 55 (2017) e163–e166, https://doi.org/10.1515/cclm-2016-0741.
[15] S.F. Wang, J. Lee, W. Wang, Y.X. Si, C. Li, T.R. Kim, J.M. Yang, S.J. Yin, G.Y. Qian, The effect of Zn^{2+} on *Pelodiscus sinensis* creatine kinase: unfolding and aggregation studies, J. Biomol. Struct. Dyn. 31 (2013) 572–590, https://doi.org/10.1080/07391102.2012.706074.
[16] W. Wang, J. Lee, Q.X. Jin, N.Y. Fang, Y.X. Si, S.J. Yin, G.Y. Qian, Y.D. Park, Effects of osmolytes on *Pelodiscus sinensis* creatine kinase: a study on thermal denaturation and aggregation, Int. J. Biol. Macromol. 60 (2013) 277–287, https://doi.org/10.1016/j.ijbiomac.2013.06.015.
[17] W. Wang, C.Y. Li, C.T. Ge, L. Lei, Y.L. Gao, G.Y. Qian, De-novo characterization of the soft-shelled turtle *Pelodiscus sinensis* transcriptome using Illumina RNA-Seq technology, J Zhejiang Univ Sci B 14 (2013) 58–67, https://doi.org/10.1631/jzus.B1200219.
[18] W. Rychlik, OLIGO 7 primer analysis software, Methods Mol. Biol. 402 (2007) 35–60.
[19] M.A. Larkin, G. Blackshields, N.P. Brown, R. Chenna, P.A. McGettigan, H. McWilliam, F. Valentin, I.M. Wallace, A. Wilm, R. Lopez, J.D. Thompson, T.J. Gibson, D.G. Higgins, Clustal W and Clustal X version 2.0, Bioinformatics 23 (2007) 2947–2948, https://doi.org/10.1093/bioinformatics/btm404.
[20] W. Wang, J. Lee, H. Hao, Y.D. Park, G.Y. Qian, Hydrogen peroxide (H_2O_2) irreversibly inactivates creatine kinase from *Pelodiscus sinensis* by targeting the active site cysteine, Int. J. Biol. Macromol. 105 (2017) 1595–1601, https://doi.org/10.1016/j.ijbiomac.2017.03.025.
[21] Y. Cai, J. Lee, W. Wang, J.M. Yang, G.Y. Qian, Effect of Cd^{2+} on muscle type of creatine kinase: inhibition kinetics integrating computational simulations, Int. J. Biol. Macromol. 83 (2016) 233–241, https://doi.org/10.1016/j.ijbiomac.2015.11.077.
[22] J. Söding, Protein homology detection by HMM-HMM comparison, Bioinformatics 21 (2005) 951–960, https://doi.org/10.1093/bioinformatics/bti125.
[23] C. Notredame, D.G. Higgins, J. Heringa, T-Coffee: a novel method for multiple sequence alignments, J. Mol. Biol. 302 (2000) 205–217.
[24] B.R. Brooks, C.L. Brooks III, A.D. Mackerell Jr., L. Nilsson, R.J. Petrella, B. Roux, Y. Won, G. Archontis, C. Bartels, S. Boresch, A. Caflisch, L. Caves, Q. Cui, A.R. Dinner, M. Feig, S. Fischer, J. Gao, M. Hodoscek, W. Im, K. Kuczera, T. Lazaridis, J. Ma, V. Ovchinnikov, E. Paci, R.W. Pastor, C.B. Post, J.Z. Pu, M. Schaefer, B. Tidor, R.M. Venable, H.L. Woodcock, X. Wu, W. Yang, D.M. York, M. Karplus, CHARMM: the biomolecular simulation program, J. Comput. Chem. 30 (2009) 1545–1614, https://doi.org/10.1002/jcc.21287.
[25] T.R. Kim, S. Oh, J.S. Yang, S. Lee, S. Shin, J. Lee, A simplified homology-model builder toward highly protein-like structures: an inspection of restraining potentials, J. Comput. Chem. 33 (2012) 1927–1935, https://doi.org/10.1002/jcc.23024.
[26] J.S. Yang, J. Kim, S. Oh, G. Han, S. Lee, J. Lee, STAP refinement of the NMR database: a database of 2405 refined solution NMR structures, Nucleic Acids Res. 40 (2012) D525–D530, https://doi.org/10.1093/nar/gkr1021.

[27] S. Jo, T. Kim, V.G. Iyer, W. Im, CHARMM-GUI: a web-based graphical user interface for CHARMM, J. Comput. Chem. 29 (2008) 1859–1865, https://doi.org/10.1002/jcc.20945.
[28] W. Im, M.S. Lee, C.L.I.I.I. Brooks, Generalized born model with a simple smoothing function, J. Comput. Chem. 24 (2003) 1691–1702, https://doi.org/10.1002/jcc.10321.
[29] S.F. Wang, Y.X. Si, Z.J. Wang, S.J. Yin, J.M. Yang, G.Y. Qian, Folding studies on muscle type of creatine kinase from *Pelodiscus sinensis*, Int. J. Biol. Macromol. 50 (2012) 981–990, https://doi.org/10.1016/j.ijbiomac.2012.02.025.
[30] Y. Cai, J. Lee, W. Wang, Y.D. Park, G.Y. Qian, Towards binding mechanism of Cu^{2+} on creatine kinase from *Pelodiscus sinensis*: molecular dynamics simulation integrating inhibition kinetics study, Protein Pept. Lett. 24 (2017) 534–544, https://doi.org/10.2174/0929866524666170227122706.
[31] M.D. Baldissera, C.F. Souza, G.B. Júnior, C.M. Verdi, K.L.S. Moreira, M.I.U.M. da Rocha, M.L. da Veiga, R.C.V. Santos, B.S. Vizzotto, B. Baldisserotto, *Aeromonas caviae* alters the cytosolic and mitochondrial creatine kinase activities in experimentally infected silver catfish: impairment on renal bioenergetics, Microb. Pathog. 110 (2017) 439–443, https://doi.org/10.1016/j.micpath. 2017.07.031.
[32] P. Luckoor, M. Salehi, A. Kunadu, Exceptionally high creatine kinase (CK) levels in multicausal and complicated rhabdomyolysis: a case report, Am. J. Case Rep. 18 (2017) 746–749.
[33] H.L. Zhang, X.J. Liu, B.W. Zhang, X.X. Peng, H. Li, Amphioxus CaVPT and creatine kinase are crucial immune-related molecules in response to bacterial infection and immunization, Fish Shellfish Immunol 33 (2012) 1139–1148, https://doi.org/10.1016/j.fsi.2012.08.025.
[34] Y.S. Lin, T.H. Cheng, C.P. Chang, H.M. Chen, Y. Chern, Enhancement of brain-type creatine kinase activity ameliorates neuronal deficits in Huntington's disease, Biochim. Biophys. Acta 1832 (2013) 742–753, https://doi.org/10.1016/j.bbadis.2013.02.006.
[35] K. Ugur, Y. Aydogan, A. Akgun, S. Aydin, A high creatine kinase concentration might be a sign of McArdle disease in patient with type 1 diabetes, Biochem. Insights. 12 (2019), 117862641986140. https://doi.org/10.1177/1178626419861407.